4

Water in Rocks and Minerals – Species, Distributions, and Temperature Dependences

Jun-ichi Fukuda
Tohoku University
Japan

1. Introduction

Water is ubiquitously distributed in the interior of the earth, as various forms in rocks and minerals: In rocks, aggregates of minerals, fluid water in which molecular H_2O is clustered, is trapped at intergranular regions and as fluid inclusions (e.g., Hiraga et al., 2001). In minerals, water is located as the form of –OH in their crystal structures as impurities. Surprisingly, such water species are distributed over five times in the earth's interior than ocean water (e.g., Jacobsen & Van der Lee, 2006), and play very important roles on earth dynamics such as deformation and reactions of minerals and rocks (e.g., Thompson & Rubie, 1985; Dysthe & Wogelius, 2006). In the filed of earth sciences therefore, people are trying to measure properties of water in rocks and minerals such as species, contents, distribution, thermal behaviour, migration rate, etc.

Infrared (IR) spectroscopy is a powerful tool to quantitatively measure these properties of water in rocks and minerals (See Aines & Rossman, 1984; Keppler & Smyth, 2006 for IR spectra of various rocks and minerals). In this chapter, for an advanced IR spectroscopic measurement, I introduce in-situ high temperature IR spectroscopy to investigate above matters. First, I use chalcedonic quartz, which contains fluid water at intergranular regions and –OH in quartz crystal structures. Next, I use beryl, a typical cyclosilicate which contains isolated (not clustered) H_2O molecules in open cavities of the crystal structure. Changes of the states of water in chalcedonic quartz and beryl by temperature changes and dehydration will be discussed. Finally, I perform two-dimensional IR mappings for naturally deformed rocks to investigate water distribution in polymineralic mixtures, and discuss possible water transportation during rock deformation.

2. Methods

Transmitted IR spectra for rocks and minerals are generally measured by making thin sections of samples with thicknesses of from 20 to 200 μm, which depend on concentrations and absorption coefficients based on Beer-Lambert law. A Fourier Transform IR microspectrometer totally used in this study is equipped with a silicon carbide (globar) IR source and a Ge-coated KBr beamsplitter. IR light through a sample is measured using a mercury-cadmium-telluride detector.

In-situ high temperature IR spectra were measured for a sample on a heating stage which was inserted into the IR path. The sample was heated at 100 °C/minute to desired

temperature, and spectra were collected at about 1 minute. Mapping measurements were carried out using an auto XY-stage under atomospheric condition.

3. Water in rocks: As an example of chalcedonic quartz

Fluid water and –OH are trapped in chalcedonic quartz, an aggregate of microcrystalline quartz (SiO_2) grains (sometimes called as chalcedony or agate which has different transparency and is treated as a gem). Fluid water in chalcedonic quartz is dominantly trapped at intergranular regions such as grain boundaries and triple junctions of grains. IR spectra of chalcedonic quartz have been measured at room temperature (RT) (Frondel, 1982; Graetsch et al., 1985). In this section, I measure in-situ high temperature IR spectra for chalcedonic quartz as a representative material that abundantly contains fluid water and structurally-trapped –OH.

3.1 Typical IR spectrum at RT and water species

Figure 1 is a typical IR spectrum at RT for a thin section (ca. 100 μm thickness) of chalcedonic quartz. The band due to fluid water shows an asymmetric broad band ranging from 2750 to 3800 cm^{-1} with a shoulder around 3260 cm^{-1}: this band feature is the same with that of simple fluid water which exists everywhere around us (e.g., Eisenberg & Kauzman, 1969). –OH in chalcedonic quartz is mainly trapped as Si-OH by breaking the network of SiO_2 bonds (Kronenberg & Wolf, 1990), and the OH stretching band is sharp (3585 cm^{-1} at RT). The bending mode of fluid water, which should be seen at around 1600 cm^{-1}, is hindered by many sharp Si-O stretching bands. Combination modes of the stretching and bending modes of fluid water and Si-OH are clearly seen for a thicker sample (1 mm in Fig. 1), and they are detected at 5200 cm^{-1} and 4500 cm^{-1} respectively. Contents of fluid water and Si-OH can be calculated from these bands' heights using their molar absorption coefficients of 0.761 and 1.141 L mol^{-1} cm^{-1}, respectively (Scholze, 1960; Graetsch et al., 1985); in this case 0.32 wt % H_2O and 0.28 wt % Si-OH, respectively (Fukuda et al., 2009a).

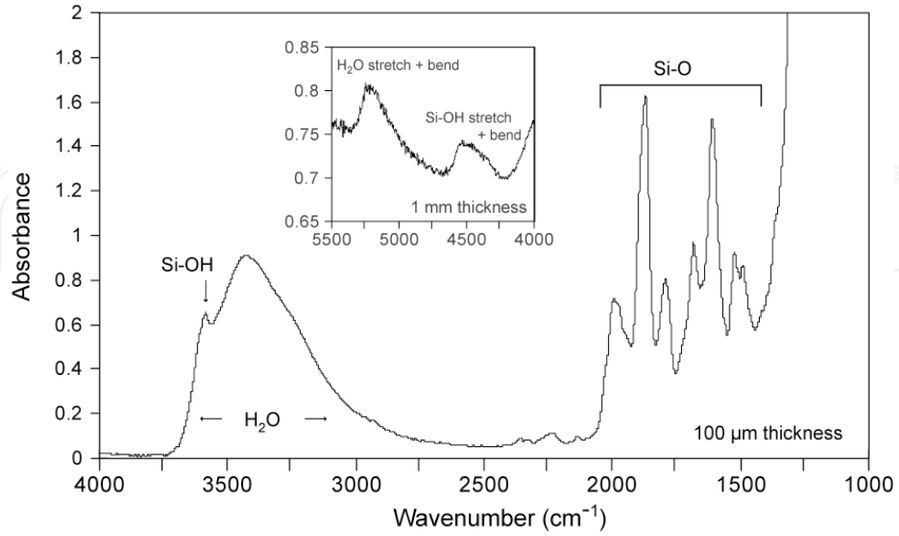

Fig. 1. Typical IR spectrum of chalcedonic quartz at RT. The sample thickness of 100 μm for 4000–1000 cm^{-1} and 1 mm for 5500–4000 cm^{-1} (combination modes of the stretching and bending modes of fluid water and Si-OH).

3.2 Water vibrations at high temperatures

High temperature IR spectra were measured for the sample set on the heating stage (Fig. 2). With increasing temperature up to 400 °C, the broad band due to fluid water dominantly and asymmetrically shifts to high wavenumbers. Contrary to this, the band due to Si-OH slightly shifts to high wavenumbers. After quenching to RT from high temperatures, these water bands do not change from those before heating, indicating that vibrational states of fluid water and Si-OH are changed at high temperatures without dehydration. The following is discussion for changes in the vibrational states of water.

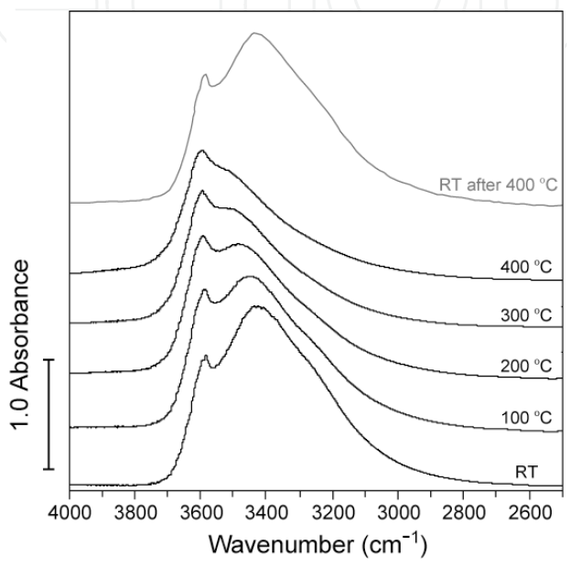

Fig. 2. In-situ high temperature IR spectra of a chalcedonic quartz (black lines) in the water stretching region (Replotted from Fukuda et al., 2009c). The spectrum at RT after heating at 400 °C is shown as gray line on the top, showing no significant change from the spectrum before heating.

Since vibrational energy of OH stretching of Si-OH is structurally limited within quartz crystal structures, the band is sharp even at high temperatures. The deviation of the wavenumber from free -OH stretching (around 3650 cm^{-1}; summarized in Libowitzky, 1999) can be explained by the work of hydrogen bond in Si-OH…O-Si in quartz crystal structures, which weaken OH vibrational energy. With increasing temperature, the hydrogen bond distance is extended due to thermal expansion of quartz crystal structure (e.g., Kihara, 2001). Resultantly, the band due to Si-OH slightly shifts to high wavenumber and the band height is not so decreased (3599 cm^{-1} at 400 °C; Fukuda & Nakashima, 2008).

In fluid water, H_2O is clustered and networked by various hydrogen bond strengths (e.g., Brubach et al., 2005). Therefore, fluid water shows the broad band. With increasing temperatures, the average coordination numbers of a H_2O molecule to adjacent H_2O molecules at confined intergranular regions of chalcedonic quartz are reduced due to increases of vibrational energies without dehydration. The average coordination number of a single H_2O molecule in fluid water is 2–3 molecules at RT (Brubach et al., 2005), and 1–2 above supercritical temperature (Nakahara et al., 2001). This leads to significant shifts of wavenumbers to higher. Also, band heights of fluid water are decreased with increasing

temperatures. For example, the maximum band height at 400 °C is approximately 50 % of that at RT. This is also because of decreases of average numbers of H_2O in areas that IR light captures (i.e., density; Schwarzer et al., 2005).

3.3 Dehydration behaviour

When the sample is kept at high temperatures, dehydration occurs. High temperature IR spectra were continuously measured to monitor dehydration. Figure 3 shows dehydration behaviour measured at 500 °C (Fig. 3a) and 400 °C (Fig. 3b). Both of the experiments were performed by heating during 500 minutes in total. Broad bands around 3800-3000 cm^{-1} in both spectra decrease with keeping at high temperatures, and the wavenumbers of the broad bands are not changed during heating. IR spectra at RT after heating (gray spectra in Fig. 3) also show decreases of fluid water. This indicates that fluid water was dehydrated through intergranular regions which are fast paths for mass transfers (See Ingrin et al., 1995; Okumura and Nakashima, 2004; Fukuda et al., 2009c for estimation of water diffusivity). Over 50 % of the band areas are decreased during the heating in 84 minutes at 500 °C. Band areas of 80 % are decreased in 250 minutes, and the features of the spectra are not changed after that. The RT temperature spectrum after 500 minutes heating at 500 °C also shows significant reduction of board band due to fluid water. This remained band due to fluid water may reflect fluid inclusions, which is tightly trapped at open spaces in crystal structures. On the other hand, 60 % of the band areas are preserved after heating in 500 minutes at 400 °C, and the RT spectrum after 500 minutes heating at 400 °C still shows a strong signal of fluid water.

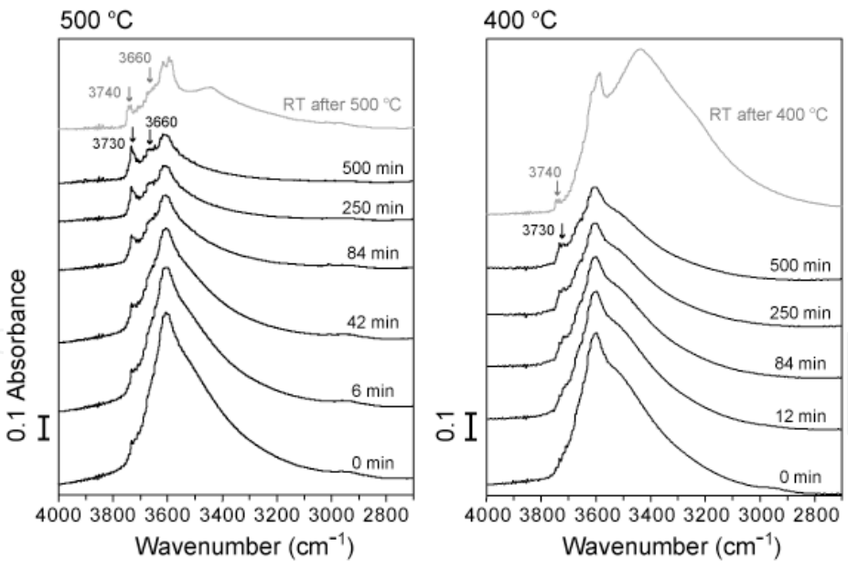

Fig. 3. Dehydration behaviour at 500 °C (left) and 400 °C (right) in the water stretching region (after Fukuda et al., 2009c). The spectra at RT after heatings are also shown as gray lines. The integrated heating times are shown at the right of each spectrum.

Since contents of fluid water are reduced by dehydration, different degrees of hydrogen bonds of Si-OH at intergranular regions (surface silanol) to fluid water are formed. This leads to the appearances of several –OH bands (3660 and 3730 cm^{-1} at 500 °C, and possibly

the split of the band at 3585 cm^{-1} at RT) (Yamagishi et al., 1997). The appearance of the band at 3730 cm^{-1} at 0 minute heating at 500 °C is due to slight dehydration during heating from RT to 500 °C at 100 °C/minute. The wavenumbers of these new –OH bands at high temperature are slightly different from those at RT, presumably due to thermal expansions of crystals and changes of hydrogen bond distances at high temperature.

4. H_2O molecules in minerals: As an example of beryl

In addition to fluid water in rocks and –OH in mineral crystal structures as described above, isolated (not clustered) H_2O molecules are incorporated in open cavities of crystal structures, and they are sometimes coupled with cations. H_2O in open cavities has well been studied for beryl, a typical cyclosilicate (after Wood & Nassau, 1967). Ideal chemical formula of beryl is $Be_3Al_2Si_6O_{18}$, and six-membered SiO_4 rings are stacked along the crystallographic *c*-axis and make a pipe-like cavity called a channel (Fig. 4) (Gibbs et al., 1968). Isolated H_2O is trapped in the channel, and forms two kinds of orientations, depending on whether it coordinates to a cation (called type II) or not (called type I) (after Wood & Nassau, 1967). Such cations are trapped in the channels to compensate the electrical charge balances caused by Be^{2+}-Li^{+} and Si^{4+}-Al^{3+} substitutions and lacks of Be^{2+} in the crystal structure of beryl. The cations in the channels are assumed to be mainly Na^{+}, and some other alkali cations may be incorporated (Hawthorne and Černý, 1977; Aurisicchio et al., 1988; Artioli et al., 1993; Andersson, 2006). In this section, I introduce polarized IR spectra of beryl, and discuss changes of the states of type I/II H_2O in the channels by temperature changes and dehydration.

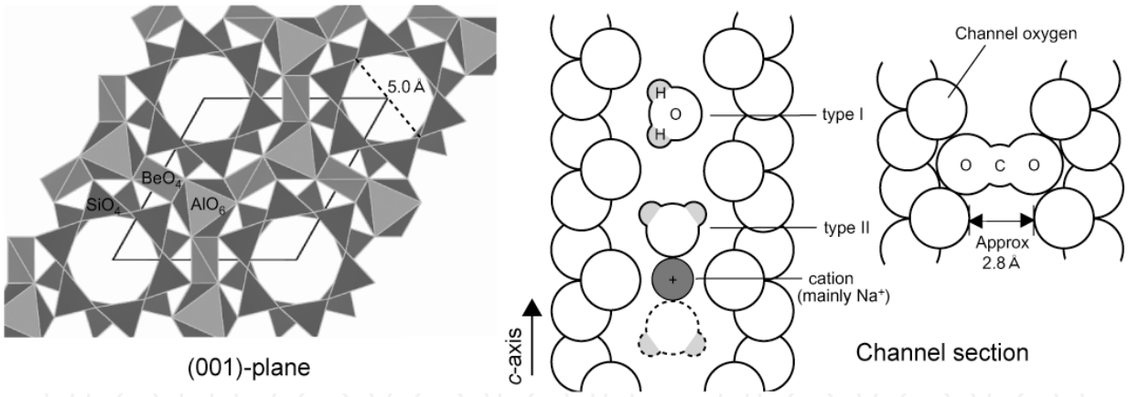

Fig. 4. Crystal structure of beryl. The (001)-plane (i.e., viewed down from the *c*-axis) and the channel section. Positions of type I/II H_2O, a cation, and CO_2 are also shown. Modified after Fukuda & Shinoda (2011).

4.1 Chemical composition of the sample

The chemical composition of the natural beryl sample used in this study was analyzed by X-ray wavelength dispersive spectroscopy for major atomic contents, inductivity coupled plasma-atomic emission spectroscopy for Be content, and atomic absorption spectroscopy for Li and Rb contents (Table 1). The type I/II H_2O contents were determined from intensities of IR bands due to the asymmetric stretching of type I and the symmetric stretching of type II in a polarized IR spectrum at RT (See the spectrum in the next section), using their molar absorption coefficients of 206 L mol^{-1} cm^{-1} and 256 L mol^{-1} cm^{-1},

respectively (Goldman et al., 1977). The CO_2 content was also calculated for the band at 2360 cm^{-1} from 800 L mol^{-1} cm^{-1} in Della Ventura et al. (2009). In the chemical composition, the Li and Na contents are relatively high in addition to the Si, Al and Be contents of major atoms. Be content (2.893 in 18 oxygen), which is lower than the ideal composition of beryl ($Be_3Al_2Si_6O_{18}$), must be replaced by Li, and Na must be incorporated as Na^+ in the channels to compensate the electrical charge balance. However, Li^+ may be also incorporated in the channels, since the Li content is not completely explained by Be^{2+}-Li^+ substitution (e.g., Hawthorne and Černý, 1977).

	wt%		18O base
SiO_2	64.45	Si	5.961
Al_2O_3	18.01	Al	2.006
BeO	13.08	Be	2.893
MgO	0.01	Mg	0.002
FeO	0.16	Fe	0.013
TiO_2	–	Ti	–
MnO	0.02	Mn	0.002
CaO	0.01	Ca	0.001
NiO	0.01	Ni	0.001
Cr_2O_3	–	Cr	–
ZnO	0.17	Zn	0.012
Li_2O	0.50	Li	0.185
Na_2O	0.54	Na	0.097
K_2O	0.04	K	0.004
Rb_2O	0.02	Rb	0.001
H_2O			
type I	1.80		
type II	1.24		
CO_2	0.01		
total	100.08		

Table 1. Chemical composition of the beryl sample used in this study.

4.2 Typical polarized IR spectra of beryl at RT and types of H_2O

Polarized IR spectra were measured by inserting a wire grid IR polarizer to IR light through the sample. Electric vector of IR light, **E** to the *c*-axis (i.e., the direction of the arraignments of the channels) were gradually changed and spectra were obtained (Fig. 5). Fundamental vibrations of type I/II H_2O (asymmetric stretching; ν_3, symmetric stretching; ν_1, and bending modes; ν_2) can be detected under different polarized conditions, which correspond to the orientations of type I/II H_2O in the channels (Fig. 4) and IR active orientations of their vibrational modes: In a sample section of the (100)-plane (i.e., the section including the alignment of channels), the bands due to the ν_3 mode of type I (referred to as ν_3-I hereafter), ν_1-II, and ν_2-II are dominantly detected under **E**//*c*-axis (Fig. 5a). Their wavenumbers are 3698, 3597, and 1628 cm^{-1}, respectively.

Under **E**⊥*c*-axis in the (100)-section (bottom spectra in Fig. 5a) or in the (001)-section (Fig. 5b), the bands due to ν_3-II (3661 cm^{-1}), ν_1-I (3605 cm^{-1}), and ν_2-I are dominant. The ν_2-I

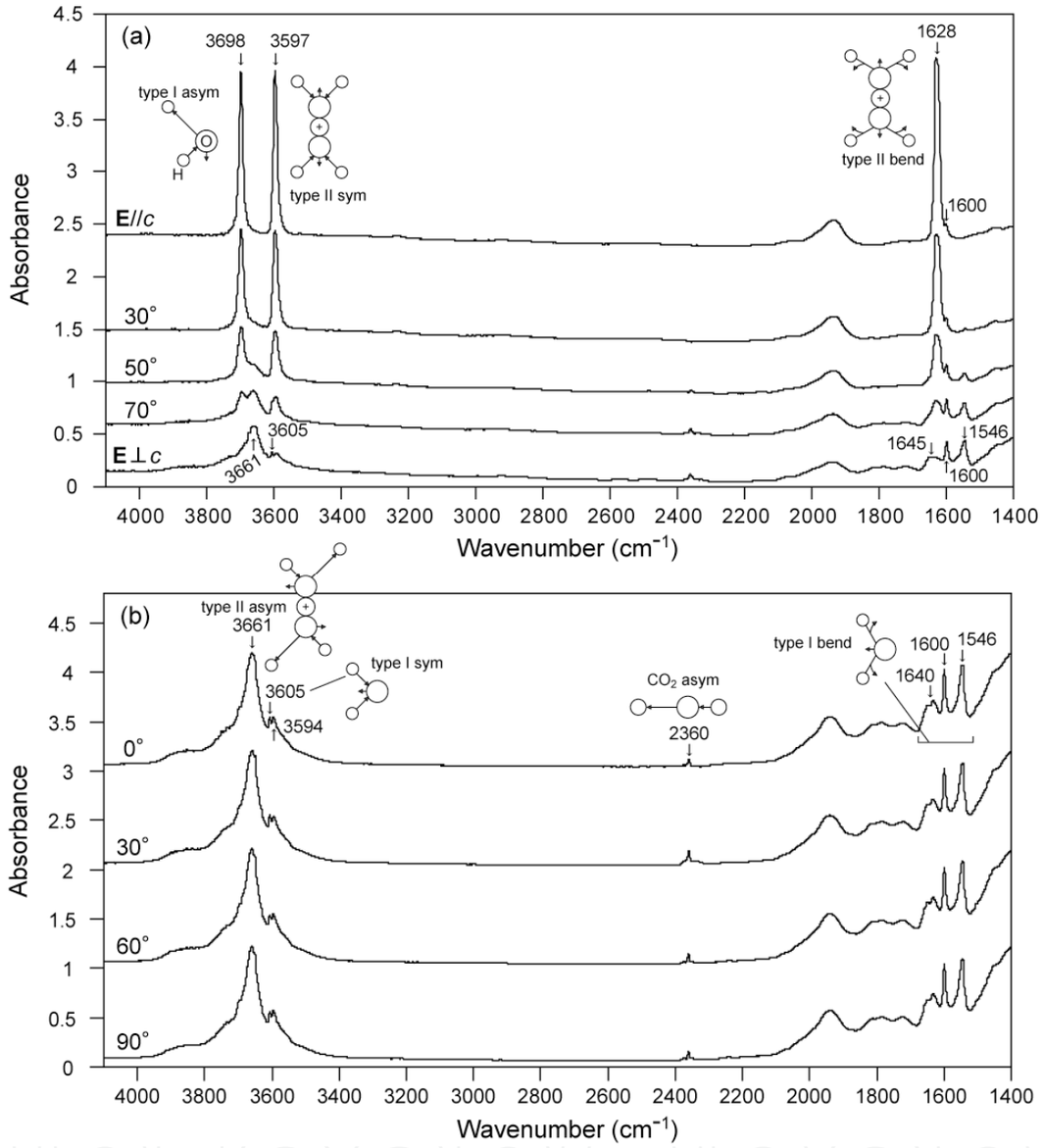

Fig. 5. Polarized IR spectra for natural beryl under different polarized conditions at RT. (a) From **E**//*c*-axis to **E**⊥*c*-axis in the (100)-section (the sample thickness of 20 μm). The angle of the *c*-axis (i.e., the direction of the channels) respective to **E** is shown on the left of each spectrum. (b) Under **E**⊥*c*-axis in the (001)-section (the sample thickness of 120 μm).

somewhat shows three bands at 1640, 1600, and 1546 cm^{-1} (e.g., Wood & Nassau 1967; Charoy et al., 1996; Łodziński et al., 2005), and I refer these three bands to the ν_2-I related bands. The asymmetric stretching mode of CO_2 molecules is detected at 2360 cm^{-1} under **E**⊥*c*-axis. These H_2O and CO_2 bands are not changed at any angles of **E** to the sample in the (001)-plane, corresponding to that these molecules are isotropically distributed due to the hexagonal symmetry of beryl. There are other unassigned bands; for example the sharp band at 3594 cm^{-1} can be seen. This band has been argued and might be due to Na^+-OH in the channels.

Ideally, the v_3, v_1, and v_2 modes of isolated free H_2O are detected at 3756, 3657, and 1595 cm^{-1}, respectively at RT (Eisenberg & Kauzman, 1969). That the fundamental vibrations of type I/II H_2O in beryl are deviated from those for ideal value, is due to interaction of type I/II H_2O with channel oxygens and cations (Fig. 5). The wavenumbers of the stretching modes of type I/II H_2O at RT are lower than those of free H_2O, while those of the bending modes are higher. Falk (1984) experimentally demonstrated reverse correlations of band shifts between stretching and bending modes. The lower wavenumbers of the stretching modes than those of isolated water molecules are due to weak hydrogen bonds between type I/II and channel oxygens, similarly to the case for chalcedonic quartz. The reverse wavenumber shifts from ideal H_2O between stretching and bending modes is mainly explained by changes in H-H repulsion constants in a simple spring model (Fukuda & Shinoda, 2008).

4.3 Water vibrations at high temperatures

Significant dehydration does not occur during short time heating from RT to 800 °C (temperature raise of 100 °C/minute and 1 minute for the measurements at each temperature; see Section 2). Figure 6 shows high temperature behaviour of type I/II H_2O in

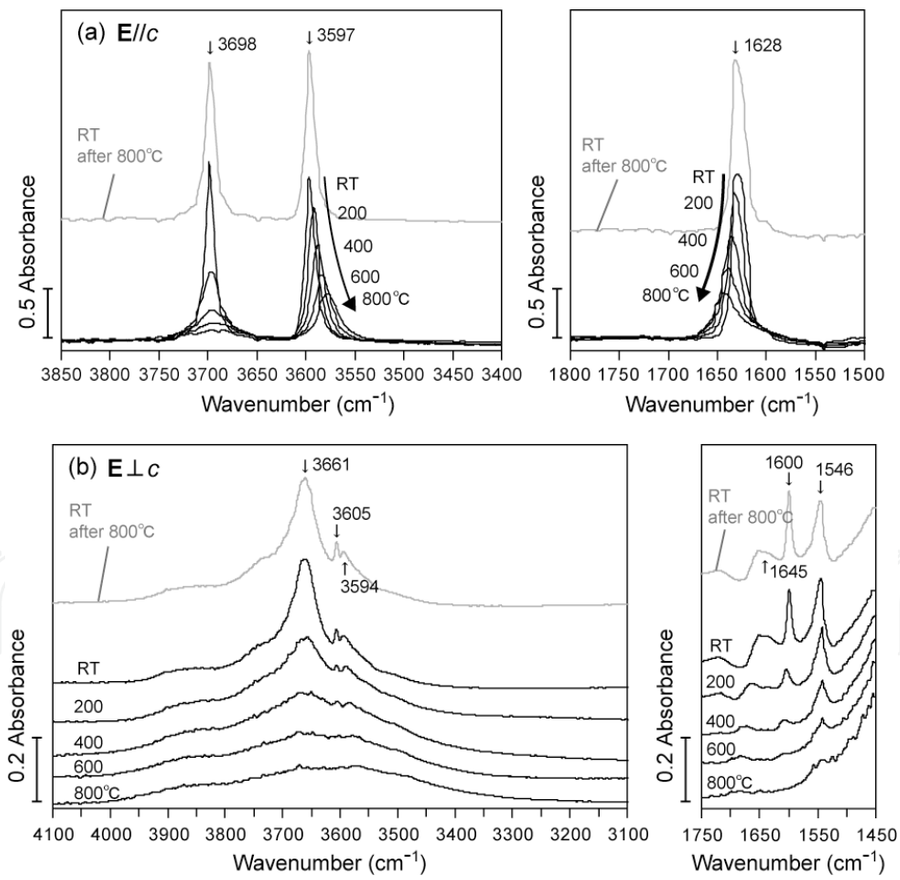

Fig. 6. High temperature behaviour of beryl from RT to 800 °C for the samples in Fig. 5 (Replotted from Fukuda & Shinoda, 2011). (a) under **E**//*c*-axis. (b) under **E**⊥*c*-axis. The RT spectra after heating at 800 °C are shown as gray lines, showing no significant dehyderation occured during heating.

beryl under **E**//*c*-axis (Fig. 6a) and **E**⊥*c*-axis (Fig. 6b) in the water stretching and bending regions. Spectral changes are different for each vibrational mode of type I/II H_2O: Under **E**//*c*-axis at RT, the ν_3-I and ν_1-II bands are clearly seen at 3698 and 3597 cm^{-1}, respectively. The ν_3-I band is rapidly decreased in its height with increasing temperature; for example 60 % of the band height decreases at 200 °C, compared with that at RT (Fig. 7). The rapid decreases of the type I band are also seen for the ν_1-I band and the ν_2-I related bands under **E**⊥*c*-axis (Fig. 6b). Contrary to the case for the type I bands, only 20 % of the ν_1-II and ν_2-II bands are decreased at 200 °C. Alternatively, wavenumber shifts dominantly occur for these bands. The wavenumber of the former (3597 cm^{-1} at RT) and latter bands (1628 cm^{-1} at RT) linearly shift to lower and higher, with increasing temperature (Fig. 7). The changes of the ν_3-II band (3661 cm^{-1} at RT) under **E**⊥*c*-axis are difficult to monitor because of overlapping with other bands at high temperatures. Since these changes are reversible upon heating and cooling, they are not due to dehydration but changes of the states of type I/II H_2O in the channels. Discussion is as follows.

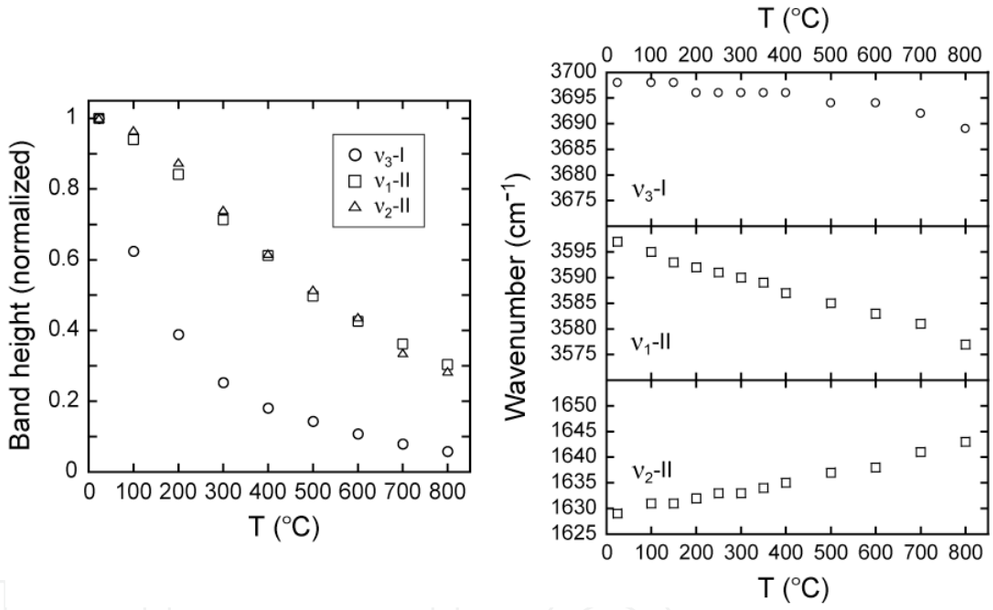

Fig. 7. Changes of band heights (left) and wavenumbers (right) of the ν_3-I, ν_1-II, and ν_2-II bands with increasing temperature (Modified after Fukuda & Shinoda, 2011). Values are determined from the spectra in Fig. 6a.

These changes in band heights and wavenumbers of type I/II H_2O are interpreted mainly due to the presence (type I) or absence of cations (type II) in the beryl channels (Fig. 4). Since type I H_2O is not coupled with a cation, its position in the channels is easy lost with increasing temperature, resulting the rapid decreases of band heights. On the other hand, since the position of type II H_2O is fixed by a cation (mainly Na^+), the decreases in band heights with increasing temperature do not significantly occur, compared with those for type I bands. Alternatively, the wavenumber shifts occur. The inverse wavenumber shifts of type II bands in stretching and bending modes would be due to modifications in vibrational constants in the thermally-expanded beryl channels (Fukuda et al., 2009b), as similar to the deviations of wavenumbers from ideal H_2O molecule in RT spectra (Section 4.2).

4.4 Dehydration behaviour

The beryl sample was heated on the heating stage at 850 °C where dehydration is enhanced (Fukuda & Shinoda, 2008). Polarized IR spectra are shown only at RT quenched from 850 °C (Fig. 8), since in-situ high temperature IR spectra at 850 °C show broadened water bands (Fig. 6) and changes of each bands are not clearly monitored. Under **E**//*c*-axis, the ν_3-I band at 3698 cm^{-1} disappeared at heating of 12 hours, without any wavenumber changes (Fig. 8a). This trend is same with the band at 3605 cm^{-1} (ν_1-I) and three ν_2-I-related bands under **E**⊥*c*-axis (Fig. 8b). Some bands remain in the water bending region under **E**⊥*c*-axis, and they would be due to structural vibrations of beryl. The dehydration behaviour of type II bands are different with that of type I: Since the position of type II H_2O is fixed by a cation, its dehydration is obviously slower than type I H_2O. Under **E**//*c*-axis, new bands develop at 3587 and 1638 cm^{-1} with decreasing of the initial bands at 3597 (ν_1-II) and 1628 cm^{-1} (ν_2-II). The band at 3661 cm^{-1} (ν_3-II) under **E**⊥*c*-axis also shows the wavenumber shifts to the lower with decreasing its intensity. These bands are stable after 24 hours heating. The appearances of these bands are explained as follows.

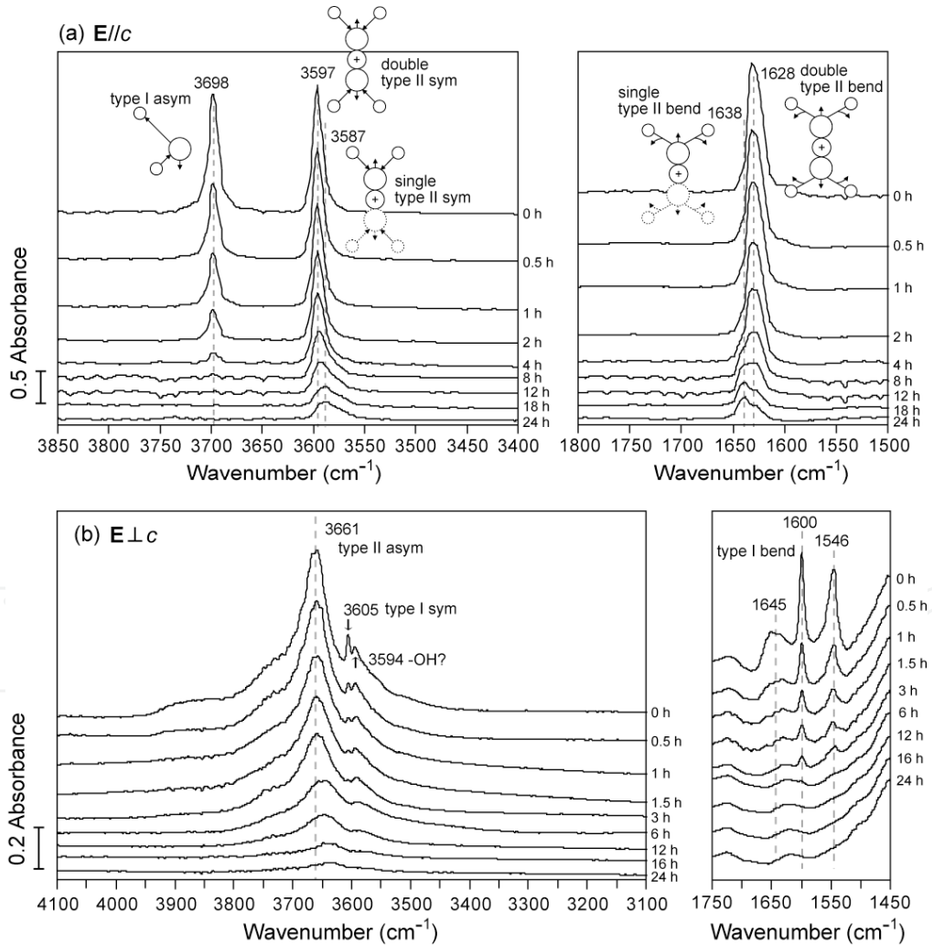

Fig. 8. IR spectra at RT quenched from heating at 850 °C, showing dehydration behaviour (Replotted from Fukuda & Shinoda, 2011). (a) under **E**//*c*-axis. (b) under **E**⊥*c*-axis. Heating times at 850 °C are shown at the right of each spectrum.

A cation is coordinated by one or two type II H_2O due to a spatial restriction of the channel (Fig. 4). Therefore, the dominant band at 3597 (ν_1-II) and 1628 cm^{-1} (ν_2-II) before heating would be mainly due to doubly-coordinated type II to a cation, mainly Na^+. Since type II H_2O dehydrates by heating, singly-coordinated type II are created. The wavenumbers of singly- and doubly-coordinated H_2O have been calculated for free H_2O molecules. According to a numerical approach for water vibrations by Bauschlicher et al. (1991), the wavenumbers of H_2O-Na^+-H_2O is higher in its stretching modes and lower in the bending modes than those of Na^+-H_2O in approximately 10 cm^{-1}. This is consistent with wavenumber shifts in beryl due to the formation of singly-coordinated type II at 3587 (ν_1-II) and 1638 cm^{-1} (ν_2-II).

Another possibility for the wavenumber shifts of the ν_1-II and ν_2-II bands is the presence of Li^+ in the channels. According to the calculation in Lee et al. (2004) for free H_2O molecules, the wavenumbers of Li^+-H_2O is higher in its stretching modes and lower in the bending modes than those of Na^+-H_2O. Also, binding energy of Li^+ to H_2O is higher than that of Na^+ to H_2O, which indicates the stable stability of Li^+-H_2O during dehydration. If Li^+ is trapped in the beryl channels, it can cause the wavenumber shifts observed in this study.

A sharp and unassigned band is seen at 3594 cm^{-1} under $\mathbf{E}\perp c$-axis. This band is also more stable than that for type I bands. The wavenumber of this band is different from any vibrational modes of type I/II H_2O. Judging from the thermal stability and the wavenumber, this band may be related to Na^+-OH in beryl, as its presence has been argued in Andersson (2006).

5. IR mapping measurements for deformed rocks

Rocks are deformed at shear zones in the interior of the earth. Rocks, which underwent brittle and plastic deformation at shear zones, are called as cataclasites and mylonites, respectively. Brittle deformation of continental crusts (mainly granitoids) is dominated from the ground to 10-20 km depth. Plastic deformation of rocks is dominated below that with increasing temperature and pressure. Another important factor that significantly contributes to plastic deformation of rocks is water. Water contents in ppm order dramatically promote plastic deformation of minerals, as confirmed by deformation experiments (e.g., Griggs, 1967; Jaoul et al., 1984; Post & Tullis, 1998; Dimanov et al., 1999). Also, water contributes to solution-precipitation which sometimes involves reactions among minerals (especially, feldspar and mica in granitoids) (e.g., summarized in Thompson & Rubie, 1985; Dysthe & Wogelius, 2006). Then, solution-precipitation creep may also contribute to the strength of the crusts (Wintsch & Yi, 2002; Kenis et al., 2005). Thus, water contents and distribution as well as its species are important for rock deformation.

In this section, I use IR spectroscopy to map two-dimensional water distributions as well as to consider its species in deformed granites. I especially focus on water distributions associated with solution-precipitation process of feldspar, and consider possible transport mechanisms of water.

5.1 Samples and analyses

Deformed granites were collected from outcrops in an inner shear zone of the Ryoke Metamorphic Belt in the Kishiwada district, Osaka Prefecture, SW Japan, and believed to be

deformed at ~500 °C (Takagi, 1988; Imon et al., 2002; 2004). Sample thin sections of ~50 μm were at first observed under a polarized optical microscope and a back-scattered electron (BSE) image which reflects compositional differences in a scanning electron microscope (SEM). After IR mapping measurements, thin sections were again polished to suitable thickness (~20 μm) to observe detailed microstructures under the optical microscope.

IR mapping measurements were carried out along ~1000 μm traverses with 30 μm spatial resolution (aperture size) in steps of 30 μm. See Section 2 for the instrument of IR spectroscopy. The integral absorbances of the water stretching bands in the range 3800–2750 cm^{-1} are displayed as a color-contoured image for a measured sample area. Color-contoured images can be used as a qualitative representation of the distribution of water, since absorption coefficients tend to increase linearly with decreasing wavenumbers (Paterson, 1982; Libowitzky & Rossman, 1997). When the absolute water contents of the minerals are to be determined, Beer–Lambert law is applied, using the absorption coefficients for each mineral. For K-feldspar and plagioclase, I used the absorption coefficients of integral water stretching bands reported by Johnson & Rossman (2003) (15.3 ppm^{-1} cm^{-2}), and for quartz, those reported by Kats (1962). Kats (1962) reported following relation between water content in quartz and integral absorbance of water stretching bands; $C(H/10^6\ Si)=0.812 \times A_{int}/d$, where A_{int} is the integral absorbance and d is the sample thickness in cm. Then, I converted $H/10^6$ Si value to a ppm H_2O unit (1 ppm = 6.67 $H/10^6$ Si), as also adopted in Gleason & DeSisto (2008). To distinguish Si-OH and H_2O contents separately, their combination bands of the stretching and bending modes should be used, as shown in Section 3. However, it is difficult for these samples, since sample thicknesses are thin for texture observations under the optical microscope, and 1 mm thickness is needed to measure the combination bands.

5.2 Typical water distribution in deformed granite

At first, I introduce water distribution in the granite mylonite with typical microtexture (Fig. 9) (See Passchier & Trouw, 2005 for many textures of deformed rocks). As can be seen under the polarized optical microscope (Fig. 9a), quartz is recrystallized by subgrain rotation, and plastically deformed by dislocation creep. Quartz grains are elongated with the aspect ratio of ca. 3:1 and the long axis is ca. 250 μm. Feldspar is a relatively hard mineral in this deformation condition, is not plastically deformed, and behaves as rigid body sometimes with fracturing (i.e., brittle deformation). Such relatively hard minerals are called as porphyroclasts. Under the BSE image, rims of plagioclase are replaced by K-feldspar, which would be due to solution-precipitation with or without reaction called myrmekitization (e.g., Simpson & Wintsch, 1989). Myrmekitization is the following reaction; K-feldspar + Na^+ + Ca^{2+} = plagioclase + quartz + K^+, where cations are included in circulating fluid water. Water contents in these replaced K-feldspar are difficult to determine in this region because of the limitation of its distribution, and discussed for other regions later.

The IR spectra for both plagioclase and quartz show broad bands at 3800–2750 cm^{-1}, which is due to the stretching vibration of fluid water (Fig. 9d) (See Section 3). Fluid water must be trapped as fluid inclusions within both minerals, since spatial resolution of 30 μm (aperture size) covers intracrystalline regions, rather than intergranular regions. The IR spectra for the plagioclase porphyroclast also exhibit sharp bands at 3625 and 3700 cm^{-1}, which are due to the stretching vibrations of structural hydroxyl in plagioclase (e.g., Hofmeister & Rossman, 1985; Beran, 1987; Johnson & Rossman, 2003). The band at 1620 cm^{-1} in plagioclase is due to

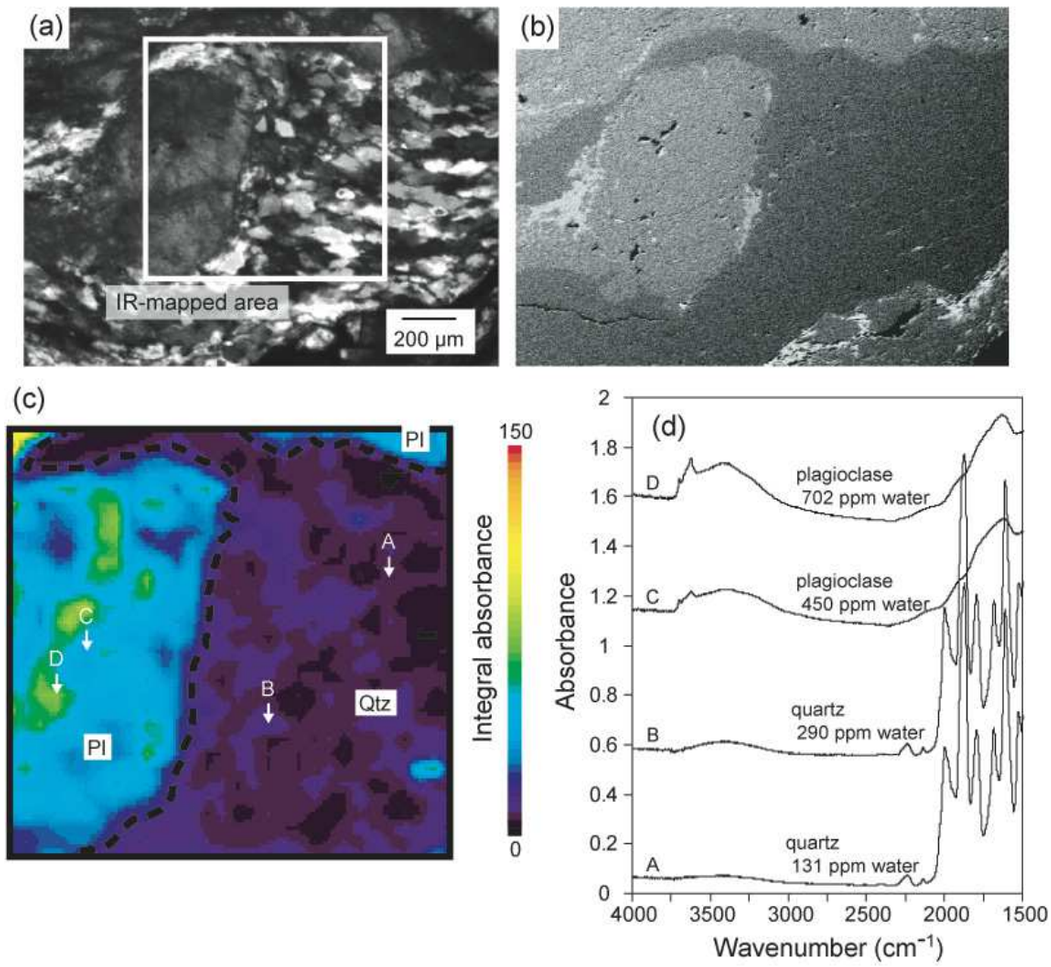

Fig. 9. (a) Optical microscopic image including the IR mapped area (bold square). (b) SEM-BSE image of the IR mapped area shown in (a): light gray; K-feldspar, medium gray; plagioclase, dark gray; quartz. (c) Water distribution mapped by integral absorbance of water stretching bands in the 3800–2750 cm^{-1} range of the IR spectra. The color contours from black to red approximately correspond to water contents from low to high. The boundaries of minerals are shown as dotted lines. Arrows with letters show the locations used to illustrate the various selected IR spectra in (d). Pl; plagioclase, Qtz; quartz.

the bending vibrations of fluid water. Other bands in the range of 2500–1500 cm^{-1} are due to the structural vibrations of plagioclase. Six sharp bands between 2000 and 1500 cm^{-1} for quartz are due to the structural vibrations of quartz, which are same with the spectra for chalcedonic quartz (Fig. 1). Recognition of the bending vibrations of fluid water in quartz is difficult because of these sharp structural bands. Water concentration in this plagioclase porphyroclast ranges from 200 to 700 ppm, with an average of 450 ppm, consistent with values reported in the literature (Hofmeister & Rossman, 1985; Beran, 1987; Johnson & Rossman, 2003). The heterogeneity of water distribution in plagioclase does not directly correspond to textures under the optical microscope and BSE. The amount of water in the quartz is much lower than that in the plagioclase, ranging from 80 to 300 ppm, with an average of 130 ppm.

5.3 Water distribution around feldspar fine grains and possible water transportation

Water distribution was measured for an area where fine-grained K-feldspar develops around K-feldspar and plagioclase porphyroclasts (Fig. 10a). The BSE image shows that fine-grained K-feldspar regions, which are constructed by ~20 μm grains, contain patchy distribution of plagioclase (Fig. 10b). This indicates that solution-precipitation of K-feldspar, which may be accompanied with myrmekitization, occurred for the development of fine grains. The IR-mapped image shows that water contents in these regions are 220 ppm H_2O in average; low and homogeneously distributed, although fluid water must be participated in the solution-precipitation process. The features of water stretching bands of fine-grained K-feldspar and K-feldspar porphyroclasts do not show structural –OH bands, differently from plagioclase (Fig. 10d); only broad bands can be seen at 3800–2750 cm^{-1}. Water contents in K-feldspar and plagioclase porphyroclasts are 200-1150 ppm; heterogeneously distributed compared with those in fine-grained K-feldspar regions.

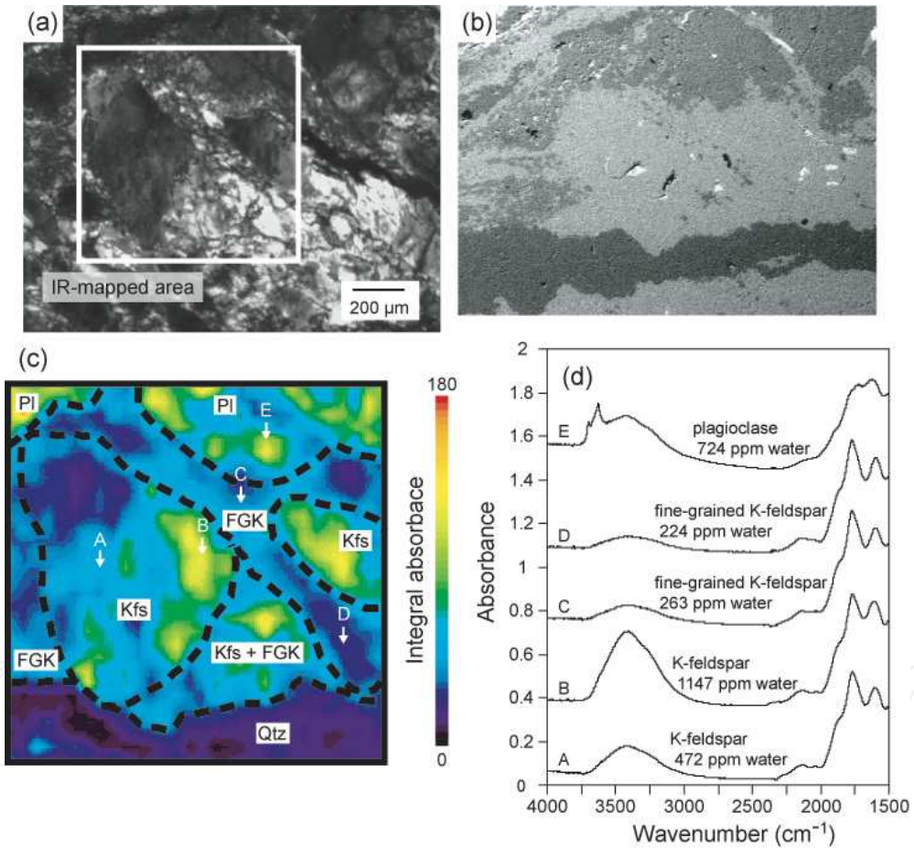

Fig. 10. (a) Optical microscopic image including the IR mapped area (bold square). (b) SEM-BSE image of the mapped area shown in (a): light gray; K-feldspar, dark gray; quartz. Fine-grained K-feldspar regions contain patchy-distributed plagioclase, indicating solution-precipitation occurred for the developments of these regions. (c) Water distribution mapped by integral absorbance of water stretching bands in the 3800–2750 cm^{-1} range of the IR spectra. The boundaries of minerals are shown as dotted lines. Arrows with letters show the locations used to illustrate the various selected IR spectra in (d). Pl; plagioclase, Kfs; K-feldspar, FGK; fine-grained K-feldspar, Qtz; quartz.

Figure 11 shows water distribution in an area that dominantly includes fine-grained plagioclase. The fine-grained plagioclase develops around plagioclase porphyroclasts, and some of it is closely associated with K-feldspar under the BSE image (Fig. 11b). Quartz in this region can be identified from its characteristic structural vibrations in the IR spectra (Fig. 11d), indicating that myrmekitization (K-feldspar + Na^+ + Ca^{2+} = plagioclase + quartz + K^+; see Section 5.2) occured during rocks deformation. Water contents in the area where fine-grained plagioclase grains are associated with small amounts of K-feldspar and quartz are roughly 2–4 times lower than those within plagioclase porphyroclasts, as inferred from the color contrasts in the IR mapping image (Fig. 11c). However, it is not possible to measure the absolute water contents in this area because of a mixture of plagioclase, K-feldspar, and quartz; consequently, the absorption coefficients are not clear.

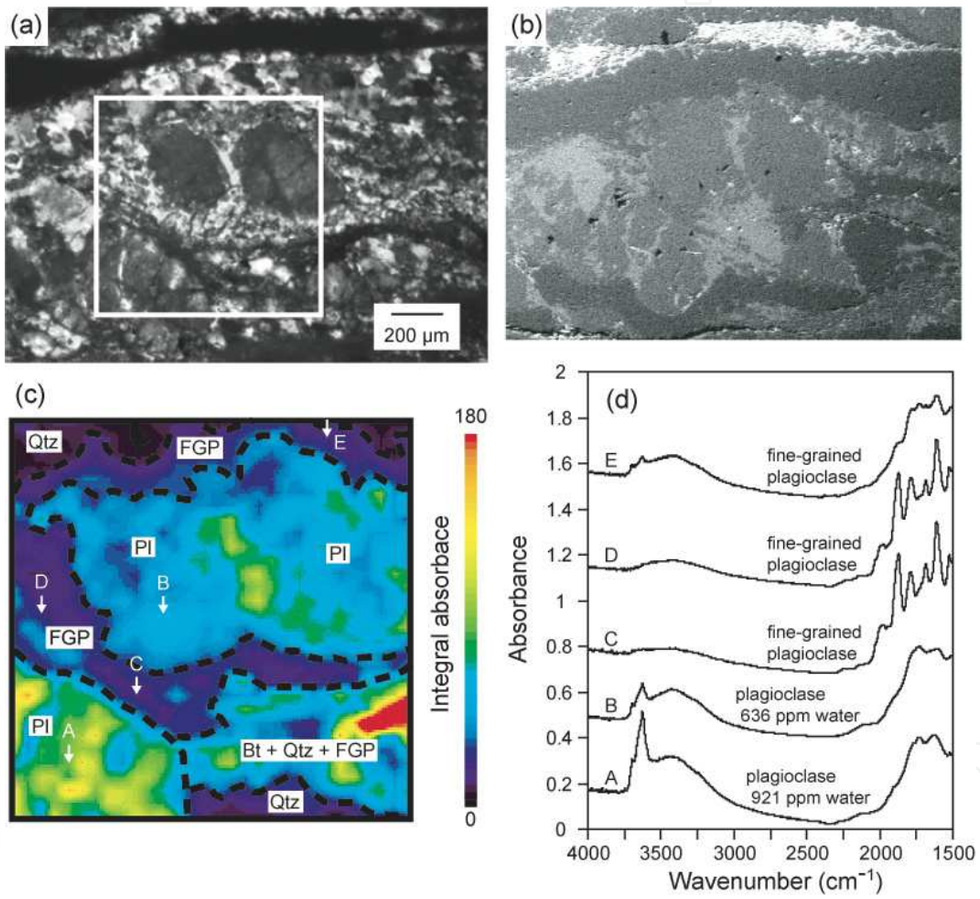

Fig. 11. (a) Optical microscopic image including the IR mapped area (bold square). (b) SEM-BSE image of the mapped area shown in (a): light gray; K-feldspar, medium gray; plagioclase, dark gray; quartz. (c) Water distribution mapped by integral absorbance of water stretching bands in the 3800–2750 cm^{-1} range of the IR spectra. The boundaries of minerals are shown as dotted lines. Arrows with letters show the locations used to illustrate the various selected IR spectra in (d). Pl; plagioclase, FGP; fine-grained plagioclase, Qtz; quartz. IR spectra show quartz vibrational bands in fine-grained plagioclase. Absolute water contents for fine-grained plagioclase are not determined due to the mixtures of quartz and K-feldspar.

In general, fluid water can be trapped at intergranular regions (grain boundaries) up to a few thousand ppm H_2O, as reported for quartz aggregates whose each grain size is a few tens of micrometers to a few hundred micrometers (e.g., Nakashima et al., 1995; Muto et al., 2004; O'kane et al., 2005). In this study, intergranular regions must also be covered in the measurements for fine-grained K-feldspar- and plagioclase-dominant regions. The solution-precipitation process that produces fined-grained K-feldspar and plagioclase are subsequently and/or simultaneously enhanced by the ability of fluid water along intergranular regions to carry ions in solution, especially in situations where intergranular diffusion was promoted by an increase in surface area. (e.g., Simpson & Wintch, 1989; Fitz Gerald & Stünitz, 1993; Tsurumi et al., 2003). However, contrary to the previous knowledge on water contents at intergranular regions, water contents in fine-grained K-feldspar- and plagioclase-dominant regions are low and homogeneous (av. 250 ppm). Therefore, it can be inferred that fluid water may not abundantly be trapped in newly-created grains, and rather released during and/or after the solution-precipitation process. The release of fluid water and dissolved ions, which contributed to the process, was a result of the concentration gradients formed in the context of numerous newly-created intergranular regions within the mix of fine-grained feldspar and quartz. As a consequence, the entire process results in a positive feedback to promote the solution-precipitation process.

6. Conclusions

I investigated high temperature behaviour of water in rocks and minerals. Chalcedonic quartz was used as a representative rock which contains abundant fluid water at intergranular regions and –OH in quartz crystal structures. The average coordination numbers of water molecules were degreased with increasing temperature, which causes shifts of stretching vibrations to higher wavenumbers. Dehydration of fluid water in the chalcedonic quartz was monitored by keeping at high temperatures. Fluid water was rapidly dehydrated through intergranular regions at 500 °C, and new hydroxyl bands appeared with dehydration of fluid water.

States of water molecules, which are not clustered like fluid water, were investigated for beryl, typical cyclosilicate, using high temperature polarized IR spectroscopy. The beryl channels, open cavities in the crystal structures, contain two types of water molecules which freely exist or coordinate to cations from up and/or below them. The former type of water easily looses its specific position, resulting the rapid degreases of its IR band heights without dehydration, and shows rapid dehydration at 850 °C. The latter type of water shows significant changes in its wavenumbers with increasing temperatures. There are slight modifications in the wavenumbers during dehydration due to changes of coordination to cations during dehydration.

Distribution of fluid water was measured for deformed granites. K-feldspar and plagioclase fine grains were formed around porphyroclasts by solution-precipitation process. Water contents in fine-grained K-feldspar- and plagioclase-dominant regions show low and homogeneous distribution of fluid water, while water distributions in host porphyroclasts were heterogeneous. This indicates that fluid water, which was involved in the solution-precipitation process, was released during and/or after the solution-precipitation process.

7. Acknowledgment

I thank K. Shinoda, J. Muto, T. Okudaira, and T. Hirono for their helpful comments on the manuscript. K. Shinoda is especially thanked for the advice on IR measurements and supports on sample preparation of beryl. T. Okudaira is also thanked for the supports for sample collection of the deformed rocks. This work was financially supported by a Grant-in-Aid for Scientific Research (212327) and (233694) by the Japan Society for the Promotion of Science for Young Scientists.

8. References

Aines, R.D. & Rossman, G.R. (1984). Water in minerals? A peak in infrared. *Journal of Geophysical Research,* Vol. 89, pp. 4059-4071

Andersson, L.O. (2006). The positionof H^+, Li^+ and Na^+ impurities in beryl. *Physics and Chemistry of Minerals*, Vol. 33, pp. 403-416

Artioli, G., Rinaldi, R., Ståhl, K. & Zanazzi, P.F. (1993). Structure refinements of beryl by single-crystal neutron and X-ray diffraction. *American Mineralogist,* Vol. 78, pp. 762-768

Aurisicchio, C., Fioravanti, G., Grubessi, O. & Zanazzi, P.F. (1988). Reappraisal of the crystal chemistry of beryl. *American Mineralogist,* Vol. 73, pp. 826-837

Bauschlicher, C.W., Langhoff, S.R., Partridge, H., Rice, J.E. & Komornicki, A. (1991). A theoretical study of $Na(H_2O)^+_n$ (n = 1-4). *Journal of Chemical Physics*, 95, 5142-5148.

Beran, A., (1987). OH groups in nominally anhydrous framework structures: an infrared spectroscopic investigation of Danburite and Labradorite. *Physics and Chemistry of Minerals*, Vol. 14, pp. 441-445

Brubach, J.B., Mermet, A., Filabozzi, A., Gerschel, A. & Roy, A. (2005). Signatures of the hydrogen bonding in the infrared bands of water. *Journal of Chemical Physics*, Vol. 122, Article No. 184509

Charoy, B., de Donato, P., Barres, O. & Pinto-Coelho, C. (1996). Channel occupancy in an alkali-poor beryl from Serra Branca (Goias, Brazil): spectroscopic characterization. *American Mineralogist*, Vol. 81, pp. 395-403

Della Ventura, G., Bellatreccia, F., Cesare, B., Harley, S. & Piccinini, M. (2009). FTIR microspectroscopy and SIMS study of water-poor cordierite from El Hoyazo, Spain: application to mineral and melt devolatilization. *Lithos*, Vol. 113, pp. 498-506

Dimanov, A., Dresen, G., Xiao, X., & Wirth, R. (1999). Grain boundary diffusion creep of synthetic anorthite aggregates: the effect of water. *Journal of Geophysical Research*, Vol. 104, pp. 10483-10497

Dysthe, D.K. & Wogelius, R.A. (2006). Confined fluids in the Earth's crust – Properties and processes. *Chemical Geology*, Vol. 230, pp. 175-181

Eisenberg, D. & Kauzman, W. (1969). *The Structure and Properties of Water,* Oxford University Press, Oxford

Falk, M. (1984). The frequency of the H–O–H bending fundamental in solids and liquids. *Spectrochimica Acta*, Vol. A40, pp. 43-48

Fitz Gerald, J.D. & Stünitz (1993). Deformation of granitoids at low metamorphic grade. I: reactions and grain size reduction. *Tectonophysics*, Vol. 221, pp. 269-297

Frondel, C. (1982). Structural hydroxyl in chalcedony (Type B quartz). *American Mineralogist*, Vol. 67. pp. 1248-1257

Fukuda, J. & Shinoda, K. (2008). Coordination of water molecules with Na^+ cations in a beryl channel as determined by polarized IR spectroscopy. *Physics and Chemistry of Minerals*, Vol. 35, pp. 347-357

Fukuda, J. & Nakashima, S. (2008). Water at high temperatures in a microcrystalline silica (chalcedony) by in-situ infrared spectroscopy: physicochemical states and dehydration behavior. *Journal of Mineralogical and Petrological Sciences*, Vol. 103, pp. 112-115

Fukuda, J., Peach, C.J., Spiers, C.J. & Nakashima, S. (2009a). Electrical impedance measurement of hydrous microcrystalline quartz. *Journal of Mineralogical and Petrological Sciences*, Vol. 104, pp. 176-181

Fukuda, J., Shinoda, K., Nakashima, S., Miyoshi, N. & Aikawa, N. (2009b). Polarized infrared spectroscopic study of diffusion of water molecules along structure channels in beryl. *American Mineralogist*, Vol. 94, pp. 981-985

Fukuda, J., Yokoyama, T. & Kirino, Y. (2009c). Characterization of the states and diffusivity of intergranular water in a chalcedonic quartz by high temperature in-situ infrared spectroscopy. *Mineralogical Magazine*, Vol. 73, pp. 825-835

Fukuda, J. & Shinoda, K. (2011). Water molecules in beryl and cordierite: high-temperature vibrational behavior, dehydration, and coordination to cations. *Physics and Chemistry of Minerals*, Vol. 38, pp. 469-481

Gibbs, G.V., Breck, D.W. & Meagher, E.P. (1968). Structural refinement of hydrous and anhydrous synthetic beryl, $Al_2(Be_3Si_6)O_{18}$ and emerald, $Al_{1.9}Cr_{0.1}(Be_3Si_6)O_{18}$. *Lithos*, Vol. 1, pp. 275-285

Gleason, G.C. & DeSisto, S. (2008). A natural example of crystal-plastic deformation enhancing the incorporation of water into quartz. *Tectonophysics*, Vol. 446, pp. 16-30

Goldman, D.S. & Rossman, G.R. (1977). Channel constituents in cordierite. *American Mineralogist*, Vol. 62, pp. 1144-1157

Graetsch, H., Flörke, O.W. & Miehe, G. (1985). The nature of water in chalcedony and opal-C from Brazilian agate geodes. *Physics and Chemistry of Minerals*, Vol. 12, pp. 300-306

Grigss, D.T. (1967). Hydrolytic weakening of quartz and other silicates. *Geophysical Journal of the Royal Astronomical Society,* Vol. 14, pp. 19-32

Hawthorne, F.C. & Černý, P. (1977). The alkali-metal positions in Cs-Li beryl. *Canadian Mineralogist,* Vol. 15, pp. 414-421

Hiraga, T., Nishikawa, O., Nagase, T. & Akizuki, M. (2001). Morphology of intergranular pores and wetting angles in pelitic schists studied by transmission electron microscopy. *Contributions to Mineralogy and Petrology*, Vol. 141, pp. 613-622

Hofmeister, A.M. & Rossman, G.R. (1985). A model for the irradiative colaration of smoky feldspar and the inhibiting influence of water. *Physics and Chemistry of Minerals*, Vol. 12, pp. 324-332

Imon, R., Okudaira, T. & Fujimoto, A. (2002). Dissolution and precipitation processes in deformed amphibolites: an example from the ductile shear zone of the Ryoke metamorphic belt, SW Japan. *Journal of Metamorphic Geology*, Vol. 20, pp. 297-308

Imon, R., Okudaira, T. & Kanagawa, K. (2004). Development of shape- and lattice-preferred orientations of amphibole grains during initial cataclastic deformation and subsequent deformation by dissolution-precipitation creep in amphibolites from the Ryoke metamorphic belt, SW Japan. *Journal of Structural Geology*, Vol. 26, pp. 793-805

Ingrin, J., Hercule, S. & Charton, T. (1995). Diffusion of hydrogen in diopside: results of dehydration experiments. *Journal of Geophysical Research*, Vol. 100, pp. 15489-15499

Jacobsen, S.D. & Van der Lee, S. (2006). *Earth's Deep Water Cycle*, Geophysical Monograph Series, Vol. 168, American Geophysical Union, Washington, D.C.

Jaoul, O. (1984). Sodium weakening of Heavitree quartzite: preliminary results. *Journal of Geophysical Research*, Vol. 89, pp. 4271-4280

Johnson, E. & Rossman, G.R. (2003). The concentration and speciation of hydrogen in feldspars using FTIR and ^{1}H MAS NMR spectroscopy. *American Mineralogist*, Vol. 88, pp. 901-911

Kats, A. (1962). Hydrogen in alpha quartz. *Philips Research Report*, Vol. 17, pp. 1-31, 133–195, 201-279

Kenis, I., Urai, J.L., Van der Zee, W., Hilgers, C. & Sintubin, M. (2005). Rheology of fine-grained siliciclastic rocks in the middle crust−evidence from structural and numerical analysis. *Earth and Planetary Science Letters*, Vol. 233, pp. 351-360

Keppler, H. & Smyth, J.R. (2006). *Water in Nominally Anhydrous Minerals,* Reviews in Mineralogy and Geochemistry, Vol.62, The Mineralogical Society of America

Kihara, K. (2001). Moleclar dynamics interpretation of structural changes in quartz, *Physics and Chemistry of Minerals*, Vol. 28, pp. 365-376

Kronenberg, A.K. & Wolf, G.H. (1990). Fourier transform infrared spectroscopy determinations of intragranular water content in quartz-bearing rocks: implications for hydrolytic weakening in the laboratory and within the earth, *Techtonophysics,* Vol. 172, pp. 255-271

Lee, H.M., Tarakeshwar, P., Park, J., Kołaski, M.R., Yoon, Y.J., Yi, H.B., Kim, W.Y. & Kim, K.S. (2004). Insights into the structures, energetics, and vibrations of monovalent cation-$(water)_{1–6}$ clusters. *Journal of Physical Chemistry A*, Vol. 108, pp. 2949-2958

Libowitzky, E. & Rossman, G.R. (1997). An IR absorption calibration for water in minerals. *American Mineralogist,* Vol. 82, pp. 1111-1115

Łodziński, M., Sitarz, M., Stec, K., Kozanecki, M., Fojud, Z. & Jurga, S. (2005). ICP, IR, Raman, NMR investigations of beryls from pegmatites of the Sudety Mts. *Journal of Molecular Structure*, Vol. 744, pp. 1005-1015

Muto, J., Nagahama, H., & Hashimoto, T. (2004). Microinfrared reflection spectroscopic mapping: application to the detection of hydrogen-related species in natural quartz. *Journal of Microscopy-Oxford*, Vol. 216, pp. 222-228

Nakahara, M., Matubayasi, N., Wakai, C. & Tsujino, Y. (2001). Structure and dynamics of water: from ambient to supercritical. *Journal of Molecular Liquids*, Vol. 90, pp. 75-83

Nakashima, S., Matayoshi, H., Yuko, T., Michibayashi, K., Masuda, T., Kuroki, N., Yamagishi, H., Ito, Y. & Nakamura, A. (1995). Infrared microspectroscopy analysis of water distribution in deformed and metamorphosed rocks. *Tectonophysics*, Vol. 245, pp. 263-276

O'kane, A., Onasch, C.M. & Farver, J.R. (2007). The role of fluids in low temperature, fault-related deformation of quartz arenite. *Journal of Structural Geology*, Vol. 29, pp. 819-836

Okumura, S. & Nakashima, S. (2004). Water diffusivity in rhyolitic glasses as determined by in situ IR spectroscopy. *Physics and Chemistry of Minerals*, Vol. 31, pp. 183-189

Passchier, C.W. & Trouw, R.A.J. (2005). *Microtectonics (2nd Ed)*. Springer-Verlag, Heidelberg

Paterson, M.S. (1982). The determination of hydroxyl by infrared absorption in quartz, silicate glasses and similar materials. *Bulletin de Minéralogie,* Vol. 105, pp. 20-29

Post, A. & Tullis, J. (1998). The rate of water penetration in experimentally deformed quartzite: implications for hydrolytic weakening. *Tectonophysics*, Vol. 295, pp. 117-137

Schwarzer, D. (2005). Energy relaxation versus spectral diffusion of the OH-stretching vibration of HOD in liquid-to-supercritical deuterated water. *Journal of Chemical Physics*, Vol. 123, Article No. 161105

Simpson, C. & Wintsch, R.P. (1989). Evidence for deformation-induced K-feldspar replacement by myrmekite. *Journal of Metamorphic Geology*, Vol. 7, pp. 261-275

Takagi, H., Mizutani, T. & Hirooka, K. (1988). Deformation of quartz in an inner shear zone of the Ryoke belt – an example in the Kishiwada area, Osaka Prefecture. *Journal of the Geological Society of Japan,* Vol. 94, pp. 869-886 (in Japanese with English abstract).

Thompson, A.B. & Rubie, D.C. (1985). *Metamorphic Reactions, Kinetics, Textures and Deformation,* Springer, New York

Tsurumi, J., Hosonuma, H. & Kanagawa, K. (2003). Strain localization due to a positive feedback of deformation and myrmekite-forming reaction in granite and aplite mylonites along the Hatagawa Shear Zone of NE Japan. *Journal of Structural Geology*, Vol. 25, pp. 557-574

Wintsch, R.P. & Yi, R. (2002). Dissolution and replacement creep: a significant deformation mechanism in mid-crustal rocks. *Journal of Structural Geology*, Vol. 24, pp. 1179-1193

Wood, D.L. & Nassau, K. (1967). Infrared spectra of foreign molecules in beryl. *Journal of Chemical Physics,* Vol. 47, pp. 2220-2228

Yamagishi, H., Nakashima, S. & Ito, Y. (1997). High temperature infrared spectra of hydrous microcrystalline quartz, *Physics and Chemistry of Minerals*, Vol. 24, pp. 66-74

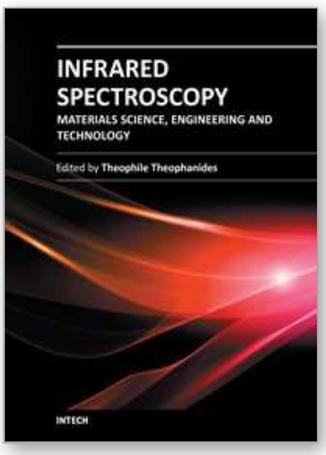

Infrared Spectroscopy - Materials Science, Engineering and Technology

Edited by Prof. Theophanides Theophile

ISBN 978-953-51-0537-4
Hard cover, 510 pages
Publisher InTech
Published online 25, April, 2012
Published in print edition April, 2012

The present book is a definitive review in the field of Infrared (IR) and Near Infrared (NIR) Spectroscopies, which are powerful, non invasive imaging techniques. This book brings together multidisciplinary chapters written by leading authorities in the area. The book provides a thorough overview of progress in the field of applications of IR and NIR spectroscopy in Materials Science, Engineering and Technology. Through a presentation of diverse applications, this book aims at bridging various disciplines and provides a platform for collaborations among scientists.

InTech Europe
University Campus STeP Ri
Slavka Krautzeka 83/A
51000 Rijeka, Croatia
Phone: +385 (51) 770 447
Fax: +385 (51) 686 166
www.intechopen.com

InTech China
Unit 405, Office Block, Hotel Equatorial Shanghai
No.65, Yan An Road (West), Shanghai, 200040, China
中国上海市延安西路65号上海国际贵都大饭店办公楼405单元
Phone: +86-21-62489820
Fax: +86-21-62489821

IntechOpen